SP Science Press

ARTICLE

Criss-cross Slip Traces During the Cyclic Deformation of Pure Coarse-Grained Polycrystalline Magnesium

Tan Li[1,3],   Huang Xingyu[1],   Sun Qi[2],   Zhang Yanbin[1],   Tu Jian[1],   Zhou Zhiming[1]

[1] College of Materials Science and Engineering, Chongqing University of Technology, Chongqing 400030, China; [2] School of Material Science and Engineering, Southwest Jiaotong University, Chengdu 610031, China; [3] Chongqing YuJiang Die-Casting Co., Ltd, Chongqing 400000, China

Abstract: The possible activated slip systems and slip traces of pure coarse-grained magnesium were investigated during cyclic deformation at room temperature. Results show that numerous criss-cross slip traces are observed on the surface of the specimens after cyclic loading. Based on the results of a combinatory analysis for the unit cell orientation and direction of the slip traces, it is determined that the criss-cross slip traces are formed by the intersection of the basal slip traces in the former matrix and the subsequent $\{10\bar{1}2\}$ twinning area during the reversed cyclic loading. Moreover, the most likely pyramidal slip mode is the sliding of $<11\bar{2}3>$ pyramidal dislocations on $\{10\bar{1}1\}$ pyramidal planes, while the basal slip traces are denser than the pyramidal slip traces, suggesting that there is limited pyramidal slip activity.

Key words: deformation twinning; magnesium; slip trace; pyramidal slip

In previous studies, activated slip modes have been identified by comparison and contrast with electron backscatter diffraction (EBSD) maps and scanning electron microscopy (SEM) images[1,2]. Obara et al[1] performed the first analysis of slip traces in magnesium. They conducted compression tests on single-crystalline magnesium at various temperatures (from room temperature to 500 °C) and observed non-basal slip traces on the adjacent faces of the single-crystalline specimens. Magnesium is a hexagonal close-packed (hcp) metal, so when a forming load is applied along its crystallographic c-axis, the non-basal slip mode is activated to accommodate the strain imposed along the c-axis[3-5]. More recently, Tang et al[6] reported that $<c+a>$ dislocations nucleate on $\{10\bar{1}1\}$ pyramidal I planes, and then slide to pyramidal II planes via cross-slip behavior. Xie et al[2] suggested that pyramidal I slip is the dominant slip mode during the c-axis compression of single-crystal magnesium at ambient temperature. In a previous study[7], the $<c+a>$ pyramidal dislocations of AZ31 magnesium were studied during cyclic deformation by transmission electron microscopy (TEM)

techniques. It was reported that such pyramidal dislocations do not form by chance, and it was concluded that this phenomenon is owed to the presence of local stress concentrations. Several studies have established that non-basal slip is of importance during the deformation of Mg and its alloys[8,9].

Fatigue occurs under cyclic loading, and the fatigue deformation mechanisms of magnesium alloy inevitably lead to complex interaction between the dislocations and twin boundaries. Koike et al[10] studied the surface of a fatigued AZ31 magnesium alloy sample after cyclic deformation, and observed the criss-cross slip traces. They ascribed this phenomenon to the cross slip between the prismatic slip system and basal slip system of the matrix. Using in-situ EBSD techniques, Yu et al[11] directly observed such criss-cross features on the surface of a single-crystal magnesium sample during cyclic deformation; they reported that the criss-cross features result from the accumulation of residual $\{10\bar{1}2\}$ twin boundaries. The kinetics of twinning-detwinning and dislocation slip behavior were observed in-situ, during the

cyclic deformation of pure coarse-grained polycrystalline magnesium[12]. Profuse slip traces were also observed on the surface of the fatigued sample. However, in the case of the aforementioned study, the formation mechanism of the criss-cross slip traces in the fatigued magnesium and its alloy is still not explicit.

Since the activations of the slip systems are closely associated with the mechanical properties of magnesium alloy, it is essential to clarify which slip systems can be activated in magnesium during cyclic deformation processes. Therefore, in the present work, we designed an experiment to analyze the slip activity that occurs during the cyclic deformation of pure magnesium at room temperature.

1 Experiment

As-cast magnesium polycrystals, with a purity of 99.98% were used. Flat dog-bone-shaped fatigue specimens were produced with gauge dimensions of 4 mm×4 mm×4 mm. The specimens were initially electrochemically polished. Subsequently, a micro area of 350 μm×350 μm, within the center of the gauge area, was selected and marked. The grains within the aforementioned marked area were observed using EBSD and SEM techniques (JOEL-JEM7800F). The loading direction of the testing specimen was aligned parallel to the normal direction (ND) of the marked grain. To further elucidate the non-basal slip systems that are active during cyclic deformation, all the cyclic tests were commenced with the application of a compressive load along the ND. The cyclic tests were performed using a MTS 809 fatigue machine at a strain amplitude of 1%; a pull-push sinusoidal loading ($R= -1$) was applied in air. The testing frequency was 0.5 Hz. In addition, EBSD observations of the structures of the marked grains were performed for the specimens that were unloaded following the first compression, the first tension, the second compression and the second tension processes. And the fatigue tests were interrupted while the EBSD images were acquired. The fatigue test was terminated immediately when the micro-cracks were initiated. To rule out the occasionality of criss-cross slip traces that were generated by cyclic loading on the sample surface, three specimens were conducted under the same fatigue test parameters as mentioned above. Similar criss-cross slip traces were observed. The surface of a sample which fatigue-failed at 196 cycles was examined using SEM to observe the slip traces in the current study.

2 Results and Discussion

2.1 Fatigue behavior

Fig.1 presents the stress-strain hysteresis loops obtained for the pure magnesium samples that were subjected to fully reversed tension-compression at a strain amplitude of 1%. The stress-strain hysteresis loops are associated with four deformation process, namely compressive loading, compressive unloading, and tensile loading, as well as tensile unloading and re-compressive loading, which occur when the strain decreases to zero. Since $\{10\bar{1}2\}$ twinning is inhibited
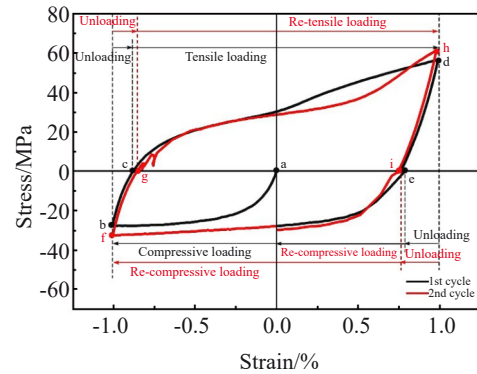

Fig.1   Stress-strain hysteresis loops in different fatigue cycles with a total strain amplitude of 1% and $R=-1$

under the *c*-axis compression, when the compressive loading (Fig. 2a and 2b) is commenced, the deformation mechanisms are accommodated by non-basal dislocation slip[13] along with possible $\{10\bar{1}1\}$ twinning[14] within the matrix. The orientation of the targeted grain is favorable for the activation of the basal slip and non-basal slip. Therefore, twinning activity is slight throughout this stage. When the compressive unloading is commenced during the first cycle (point c), detwinning occurs as soon as the load is reversed[15]. Specifically, detwinning occurs immediately; however, detwinning activity is slight during the unloading process[16]. Hama et al[17] indicated that when unloading is commenced, the activities of all systems discontinue immediately. Subsequently, the unloading process is controlled by the activity of the basal slip system at low strain; however, it is governed by both the basal slip and detwinning activities at high strains. Hence, basal slip is activated during unloading at low strains.

When the sample was loaded in tension (Fig.2c and 2d), the resultant curve exhibits a sigmoidal shape, which is characteristic of twinning behavior[18]. Twinning occurs until the sample is completely twinned at an applied strain of 1% (point d). Upon unloading from the maximum tensile stress, the twins and parents possess significant internal stress, which drives the detwinning phenomenon to occur immediately. When the sample was reloaded under compression, the detwinning was accompanied by sigmoidal-shaped compressive loading (from i to f). A significant number of asymmetric features are observed. A detwinning mechanism occurs during the reverse loading process[19]. Once the grains are completely detwinned (Fig. 2d~2g), the targeted grain is favorably oriented; once again, basal <*a*> slip and $\{10\bar{1}2\}$ twinning occur. The shapes of the subsequent hysteresis loops closely follows that obtained in the first cycle. Following the compressive unloading during the second cycle (point g), a certain degree of detwinning occurs. When the sample is reloaded in tension (from point g to h), twinning occurs again, and subsequently, detwinning continues during the subsequent loading process (from h to f).

2.2 Characteristics of microstructural evolution

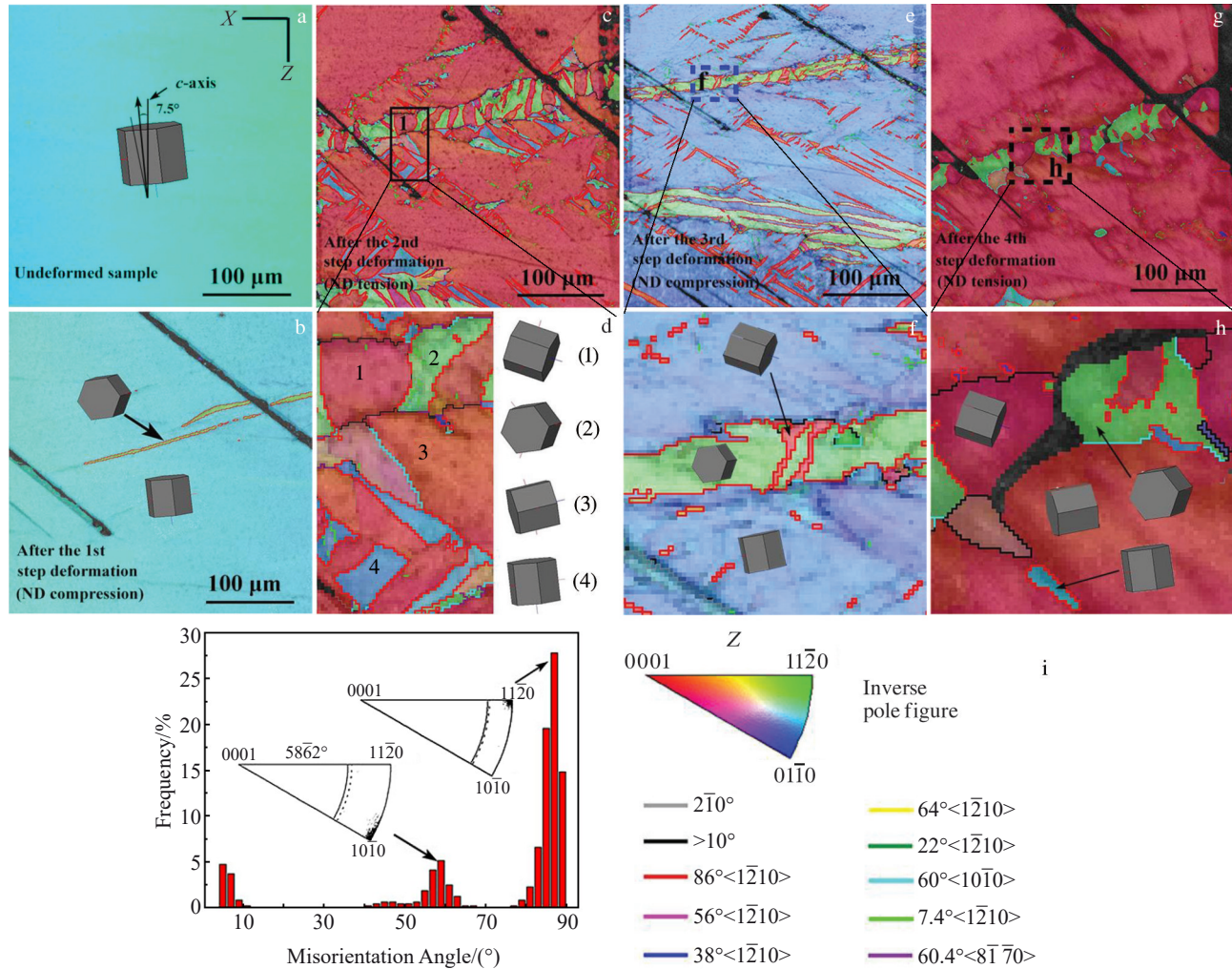Fig. 2 presents the microstructural evolution of the pure

Fig.2　EBSD images of the scanned region under various deformation steps: (a) initial sample, (b) compressed along ND, (c, d) tensed along ND, (e, f) re-compressed along ND, (g, h) re-tensed along ND, and (i) histogram of the misorientation angle distribution corresponding to Fig.2c

polycrystalline magnesium during the cyclic deformation process. The results of the EBSD analysis reveals that the actual *c*-axis of the observed grain is tilted ~7.5° from the ND of the pure polycrystalline magnesium plate. In many studies, it has been demonstrated that {10$\bar{1}$2} tensile twins, basal <a> slips, prismatic <a> slips, and pyramidal <c+a> slips are the primary deformation modes for magnesium and its alloys[20,21]. Among these deformation modes, the critical resolved shear stresses (CRSS) of {10$\bar{1}$2} tensile twins and basal <a> slips are much lower than those of other modes. Owing to their polar nature, {10$\bar{1}$2} tensile twins can be easily activated through the tensile loads parallel to the *c*-axis, or the application of compressive loads perpendicular to the *c*-axis[22]. Non-basal slips are easily activated to accommodate the *c*-axis strain when the grain is at a "hard" orientation to the active tensile twin.

The activated slip traces, and the result of the EBSD analysis of the different variants of twins are illustrated in Fig.2. Schematic unit cells are superimposed, which reveal the orientation of the matrix and the tagged twins. As shown in

Fig. 2a, the initial microstructure is twin-free. Since twinning has a polarity[23-25], the activation of the {10$\bar{1}$2} twins is limited because the *c*-axis of the grain is almost parallel to the compressive loading direction of the first-step of the deformation process. As shown in Fig. 2b, a few {10$\bar{1}$2} tension twins and slip traces, indicated by the dark arrow, can be observed. During the second step of the deformation process, the orientation of the matrix is favored for the formation of {10$\bar{1}$2} twins. As shown in Fig.2c, the nucleation and growth of {10$\bar{1}$2} twins occur readily. The twins do not require high stresses for growth, and are known to grow very rapidly consuming entire grains[26]. Once a twin is formed, the lattice within is rotated by 86°, about <1$\bar{2}$10>, with regard to the matrix[12]. To illustrate the evolution of the twins, the area with the dark-colored square in Fig. 2c is selected as a representative area for analysis. It is noted that the entire matrix is occupied by {10$\bar{1}$2} tension twins (region 3). Meanwhile, the former {10$\bar{1}$2} twins, marked by the dark arrow in Fig. 2b, grow wider and longer. In addition, new {10$\bar{1}$2} twins (region 1), with different orientations to the

matrix (region 4), also appear within the $\{10\bar{1}2\}$ primary twins (region 2). Fig. 2i presents a histogram of the misorientation angle distribution, corresponding to Fig. 2c. A low angle of 5° can be observed, which typically relates to the dislocation boundaries. The misorientation axes corresponding to the peaks at 60° and 86° are related to $< 10\bar{1}0 >$ and $< 11\bar{2}0 >$, respectively, as shown in the insets of Fig. 2i. The distribution peak at around 86° is related to the $\{10\bar{1}2\}$ tension twins (with a boundary of ~86°/$< 11\bar{2}0 >$), and the distribution peak at around 60° is related to the $\{10\bar{1}2\}$ - $\{10\bar{1}2\}$ secondary twins (with a boundary of ~60°/$< 10\bar{1}0 >$)[27]. In the present study, the $\{10\bar{1}2\}$ - $\{10\bar{1}2\}$ secondary twins are primarily recognized as $\{10\bar{1}2\}$ twins within a $\{10\bar{1}2\}$ primary twin. This is similar to the observations of previous studies[28]. They also found that such $\{10\bar{1}2\}$ - $\{10\bar{1}2\}$ secondary twins exist during the plain-strain compression of Mg.

During the third step of deformation, the primary twins and secondary twins are reduced in size; this indicates the commencement of de-twinning within the twinned area [11]. Since de-twinning leads to twin reversal, the de-twinning phenomenon is determined, upon unloading by the presence of twin boundary traces that do not conform to the ~86°/$< 11\bar{2}0 >$ misorientation. It is noteworthy that the orientation of the matrix is parallel to the $\{0002\}$ basal plane once more, as shown by the blue-colored area (Fig. 2e). In addition, many residual twins remain throughout the twinning-detwinning stage in the cyclic deformation process (as indicated by Fig. 2e); this is a very well-documented fatigue mecha-

nism[11,21]. Such residual twins provide a high density of nucleation sites during subsequent deformation. Upon the reversal of the loading, during the fourth step of deformation, twins start to reappear from the former twinned-detwinned sites (Fig. 2g). It is noted that following the application of the cyclic loading, the $\{10\bar{1}1\}$ twins can hardly be observed; this suggests that $\{10\bar{1}1\}$ twinning is not the primary deformation mode during the cyclic deformation of pure magnesium at ambient temperature.

2.3 Activated slip systems

Following the deformation process, the activated slip systems after deformation process were identified via slip trace analysis, using SEM images[12,29,30]. Fig. 3 shows the slip traces obtained after the first and the second step of deformation. A schematic of the unit lattice cells is shown to provide a better visual indication of the crystal orientation. All the slip traces exhibit typical planar slip features; for instance, the basal slip lines are rectilinear and parallel to the $\{0001\}$ basal planes; the pyramidal I slip lines are parallel to the $\{10\bar{1}1\}$ pyramidal planes; and the pyramidal II slip lines are parallel to the $\{10\bar{2}2\}$ pyramidal planes[31]. In the first step of deformation, the stress axis is almost perpendicular to the basal plane of the marked grain. Amongst all the slip systems, the basal slips exhibit the lowest CRSS at room temperature. It is also known that the CRSS of pyramidal slip is very high; this can become an important deformation mode, accommodating the strain during high-temperature deformation[13].
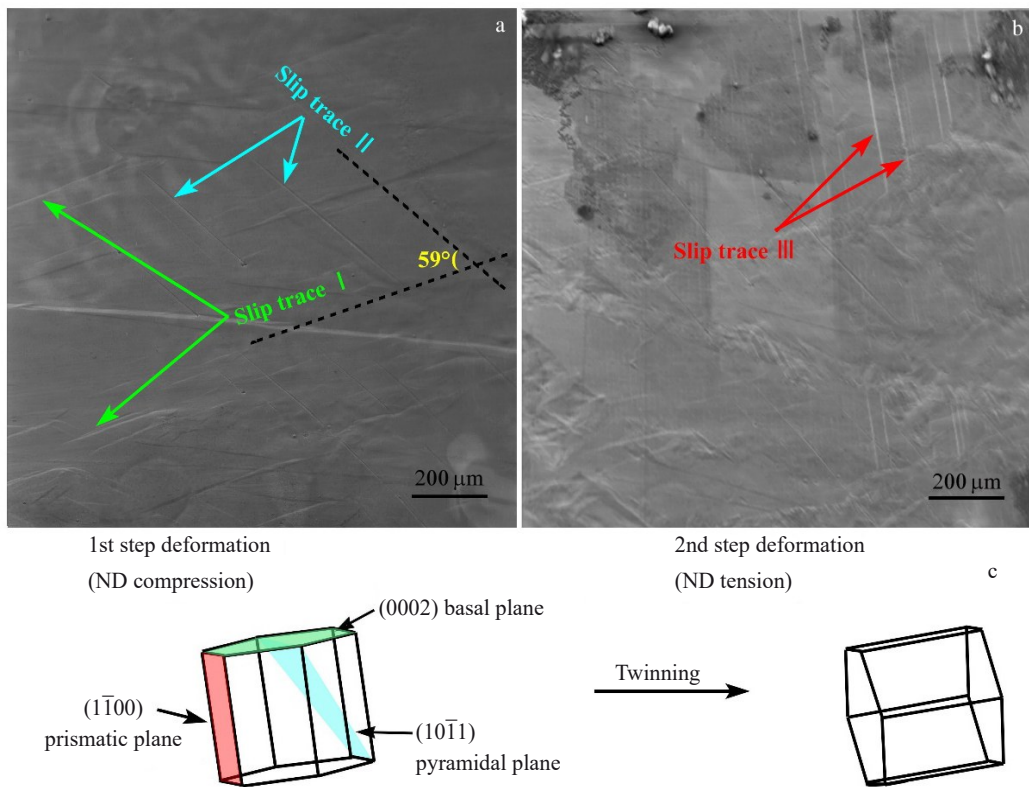

Fig.3　SEM images of the pure, coarse-grained, polycrystalline magnesium sample subjected to cyclic loading: (a) 1st step deformation; (b) 2nd step deformation; (c) schematic of the unit lattice cells
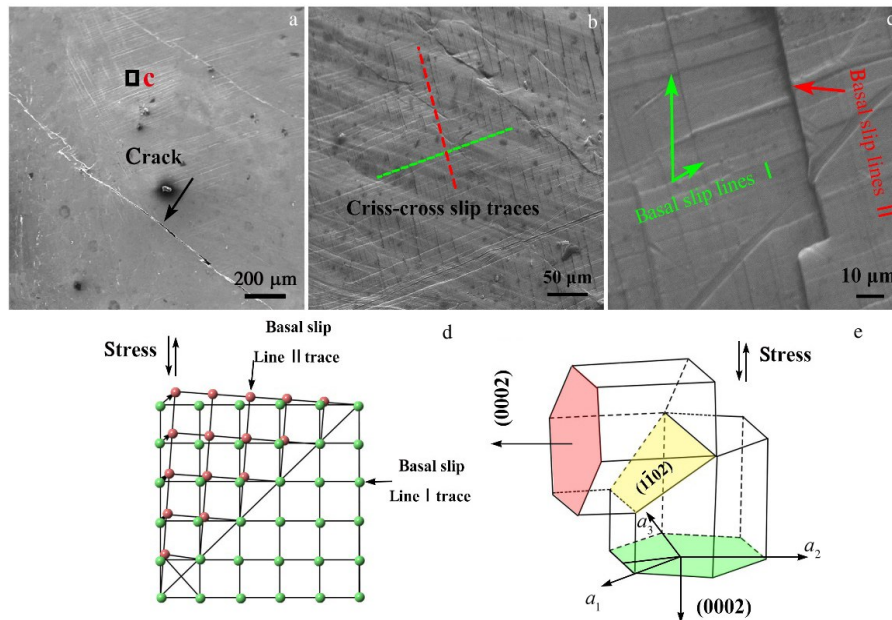
Fig.4 Cracks and fracture surfaces of the pure, coarse-grained, polycrystalline magnesium sample that was subjected to cyclic deformation: (a) crack-fracture morphology, (b) typical criss-cross slip traces, (c) magnitude of criss-cross slip traces, (d) movement of atoms forming basal slip lines I and basal slip lines II, and (e) activation of the twins on the plane with respect to compression along basal plane

Therefore, the basal slip system is easily activated in the current study. The basal slip traces in the direction indicated by the green arrows in Fig. 3a are classified as "slip traces I". It is noteworthy that several slip traces are not parallel to the basal planes; these slip traces are classified as "slip traces II", as indicated by the blue arrows. The angle between these slip traces and the basal slip traces is determined to be 59°, which is close to the theoretical angle (58°) between the (0002) basal slip and $(10\bar{1}1)$ pyramidal I plane, as viewed along the $[10\bar{1}0]$ direction[2]. Based on the results of the slip trace analysis, these slip traces are probably due to the pyramidal I slips. During the second step of deformation, the matrix is rotated by almost 90° because of $\{10\bar{1}2\}$ twinning. Another type of slip trace is also observed, denoted as "slip traces III"; it is highly likely that these will be activated in the twinned area, as indicated by the red arrows in Fig. 3b. A comparison of Fig. 3b and the crystal orientation indicates that the slip traces are parallel to the directions of the basal <a> on the basal plane, suggesting the activation of basal slip in the twinned area.

Based on the SEM observation, significant accumulation of the slip traces occurs on the surface of the sample as the number of loading cycles increases. A SEM image of the surface of the specimen, captured near the macroscopic fracture zone, is presented in Fig. 4. Cracks form following 196 cycles at room temperature (Fig. 4a). Two sets of slip traces can be observed on the surface of the sample (Fig. 4b and 4c); in addition, there are two angles between the two sets of slip traces. The high-magnification image shows that the criss-cross lines have a stepped structure (Fig. 4c). Schematic representation of atom movement is shown in Fig. 4d. In this

study, the basal slip lines I is generated by compression loading. Since the induced misorientation angle (86°) between the crystal lattice of the twinned area and the matrix is very close to 90° after the $\{10\bar{1}2\}$ twinning (Fig. 4e), the activation of basal slip II in twinned area during subsequently tension loading is highly favorable, because basal slip is the easiest slip system to activate at the room temperature[32]. Based on the SEM observation, the basal slip lines are accumulated significantly on the sample surface with increasing the loading cycles. The above analysis indicates that the final criss-cross slip traces (Fig. 4) on the surface of the sample are produced by the intersection of the basal slip traces in the matrix and the twinned area in the same region during cyclic deformation.

3 Conclusions

1) The criss-cross slip traces on the surface of the fatigued sample can be generated by the basal dislocations, which are associated with the $\{10\bar{1}2\}$ twinning behavior during the cyclic deformation process.

2) The presence of the diffuse pyramidal slip traces indicates the limited activity of the pyramidal slip systems during the cyclic deformation process.

References

1 Obara T, Yoshinga H, Morozumi S. *Acta Metallurgica*[J], 1973, 21(7): 845

2 Xie Kelvin Y, Alam Zafir, Caffee Alexander *et al. Scripta Materialia*[J], 2016, 112: 75

3 Xi Baili, Fang Gang, Xu Shiwei. *Materials Science and Engineering A*[J], 2019, 749: 148

4 Koike J, Kobayashi T, Mukai T *et al. Acta Materialia*[J], 2003, 51(7): 2055

5 Wang Fenghua, Liu Man, Sun Jie *et al. Materials Characterization*[J], 2019, 149: 118

6 Tang Yizhe, El-Awady Jaafar A. *Acta Materialia*[J], 2014, 71: 319

7 Tan Li, Zhang Xiyan, Sun Qi *et al. Materials Science and Engineering A*[J], 2017, 699: 247

8 Li Bin, Zhang Qiwei, Mathaudhu S N. *Scripta Materialia*[J], 2017, 134: 37

9 Liu Boyu, Liu Fei, Yang Nan *et al. Science*[J], 2019, 365(6448): 73

10 Koike J, Fujiyama N, Ando D *et al. Scripta Materialia*[J], 2010, 63(7): 747

11 Yu Qin, Zhang Jixi, Jiang Yanyao. *Philosophical Magazine Letters*[J], 2011, 91(12): 757

12 Vinogradov A, Vasilev E, Linderov M *et al. Materials Science and Engineering A*[J], 2016, 676: 351

13 Agnew S R, Duygulu Ö. *International Journal of Plasticity*[J], 2005, 21(6): 1161

14 Agnew S R, Brown D W, Tomé C N. *Acta Materialia*[J], 2006, 54(18): 4841

15 Wu Liang, Agnew S R, Brown D W *et al. Acta Materialia*[J], 2008, 56(14): 3699

16 Wu Baolin, Duan Guosheng, Du Xinghao *et al. Materials & Design*[J], 2017, 132: 57

17 Hama Takayuki, Kitamura Naoya, Takuda Hirohiko. *Materials Science and Engineering A*[J], 2013, 583: 232

18 Brown D W, Jain A, Agnew S R *et al. Materials Science Forum* [J], 2007, 539: 3407

19 Yu Qin, Zhang Jixi, Jiang Yanyao *et al. International Journal of Fatigue*[J], 2012, 36(1): 47

20 Li Qizhen, Yu Qin, Zhang Jixi *et al. Scripta Materialia*[J], 2010, 62(10): 778

21 Koike J, Ohyama R. *Acta Materialia*[J], 2005, 53(7): 1963

22 Huang Hongtao, Godfrey Andy, Liu Wei *et al. Materials Letters* [J], 2016, 178: 208

23 Han Tingzhuang, Huang Guangsheng, Wang Lifei *et al. Rare Metal Materials and Engineering*[J], 2020, 49(1): 21

24 Park S H, Hong S G, Lee C S. *Scripta Materialia*[J], 2010, 62(9): 666.

25 Dixit Neha, Xie Kelvin Y, Hemker K J *et al. Acta Materialia*[J], 2015, 87: 56

26 Mu Sijia, Jonas J J, Gottstein G. *Acta Materialia*[J], 2012, 60(5): 2043

27 Basu I, Al-Samman T. *Materials Science and Engineering A*[J], 2017, 707: 232

28 Wang Haozhe, Boehlert C J, Wang Qudong *et al. Materials Characterization*[J], 2016, 116: 8

29 Hou Dewen, Liu Tianmo, Chen Huicong *et al. Materials Science and Engineering A*[J], 2016, 660: 102

30 Geng J, Chisholm M F, Mishra R K *et al. Philosophical Magazine*[J], 2015, 95(35): 3910

31 Zhi Chenchen, Ma Lifeng, Huang Qingxue *et al. Rare Metal Materials and Engineering*[J], 2018, 47(5): 1555

32 Li Xianrong, Mi Yujie, Nie Huihui *et al. Rare Metal Materials and Engineering*[J], 2020, 49(1): 320

大晶粒纯镁疲劳变形过程中交叉滑移迹线的分析

谭　力[1,3]，黄星宇[1]，孙　奇[2]，张琰斌[1]，涂　坚[1]，周志明[1]

(1. 重庆理工大学 材料科学与工程学院，重庆 400030)

(2. 西南交通大学 材料科学与工程学院，四川 成都 610031)

(3. 重庆渝江压铸有限公司，重庆 400000)

摘　要：在室温条件下研究了大晶粒纯镁疲劳变形过程中有可能激活的滑移系统及滑移迹线。结果表明，经过疲劳变形后大量的纵横交叉滑移迹线在样品表面产生，基于晶粒取向与滑移迹线方向的综合判定，这种纵横交叉滑移迹线是由反复疲劳变形过程中基体的基面滑移与同一区域内｛10$\bar{1}$2｝孪生过程中所再次产生的基面滑移而形成。通过实验观察到最有可能发生的锥面滑移系统为在｛10$\bar{1}$1｝面上所产生的<11$\bar{2}$3>锥面滑移，但总体来说，基面的滑移迹线比锥面的滑移迹线更密集，这说明锥面滑移在整个疲劳变形过程中被抑制。

关键词：变形孪晶；镁；滑移迹线；锥面滑移

作者简介：谭　力，女，1985年生，博士，副教授，重庆理工大学材料科学与工程学院，重庆 400030，E-mail：tanli@cqut.edu.cn